Femtosecond photodissociation dynamics of 1,4-diiodobenzene by gas-phase X-ray scattering and photoelectron spectroscopy

Femtosecond Photodissociation Dynamics of 1,4-Diiodobenzene by Gas-Phase X-Ray Scattering and Photoelectron Spectroscopy

Brian Stankus[1], James M. Budarz[1,2], Adam Kirrander[3], David Rogers[3], Joseph Robinson[2], Thomas J. Lane[2], Daniel Ratner[2], Jerome Hastings[2], Michael P. Minitti[*2] and Peter M. Weber*[1]

[1] Dept. of Chemistry, Brown University, Providence, RI 02912, USA, E-mail: peter_weber@brown.edu

[2] SLAC National Accelerator Laboratory, Menlo Park, CA 94025, USA , E-mail: minitti@slac.stanford.edu

[3] EaStCHEM, School of Chemistry, University of Edinburgh, David Brewster Road, Edinburgh EH9 3FJ, UK

ABSTRACT

We present a multifaceted investigation into the initial photodissociation dynamics of 1,4-diiodobenzene (DIB) following absorption of 267 nm radiation. We combine ultrafast time-resolved photoelectron spectroscopy and x-ray scattering experiments performed at the Linac Coherent Light Source (LCLS) to study the initial electronic excitation and subsequent rotational alignment, and interpret the experiments in light of Complete Active Space Self-Consistent Field (CASSCF) calculations of the excited electronic landscape. The initially excited state is found to be a bound $^1B_1$ surface, which undergoes ultrafast population transfer to a nearby state in 35 ± 10 fs. The internal conversion most likely leads to one or more singlet repulsive surfaces that initiate the dissociation. This initial study is an essential and prerequisite component of a comprehensive study of the complete photodissociation pathway(s) of DIB at 267 nm. Assignment of the initially excited electronic state as a bound state identifies the mechanism as predissociative, and measurement of its lifetime establishes the time between excitation and initiation of dissociation, which is crucial for direct comparison of photoelectron and scattering experiments.

Introduction

Photodissociation reactions are ideal prototypical phenomena to explore the dynamics of unimolecular systems and the conversion of photon energy into chemical energy. Photochemical bond cleavage can occur via a variety of mechanisms, including direct promotion to a repulsive potential energy surface or predissociation after excitation to a bound state coupled to a dissociation continuum. Because they often proceed on very fast time scales, photodissociation reactions are ideally investigated using ultrafast techniques.

The photolysis of halobenzenes has been the subject of extensive experimental study[1–24], typically via analysis of photofragment energy distributions. Because of the strong coupling of the π system to a series of repulsive σ* states, their photodissociation dynamics can be quite complex. 1,4-dichlorobenzene, for example, has been shown to undergo predissociation[19], yet iodobenzene dissociates via multiple competing pathways[12,16,23]. The photodissociation of 1,4-diiodobenzene (DIB) has been observed for many years, but the mechanism, or set of mechanisms, remain largely unknown. The early photofragment studies by Bersohn *et. al.* indicated that the translational energy distribution of the iodophenyl radical did not depend on the excitation wavelength, leading those researchers to propose a predissociation mechanism[6]. No time-resolved studies of DIB have yet been reported to support that mechanism explanation or to provide time scales for the predissociation reaction.

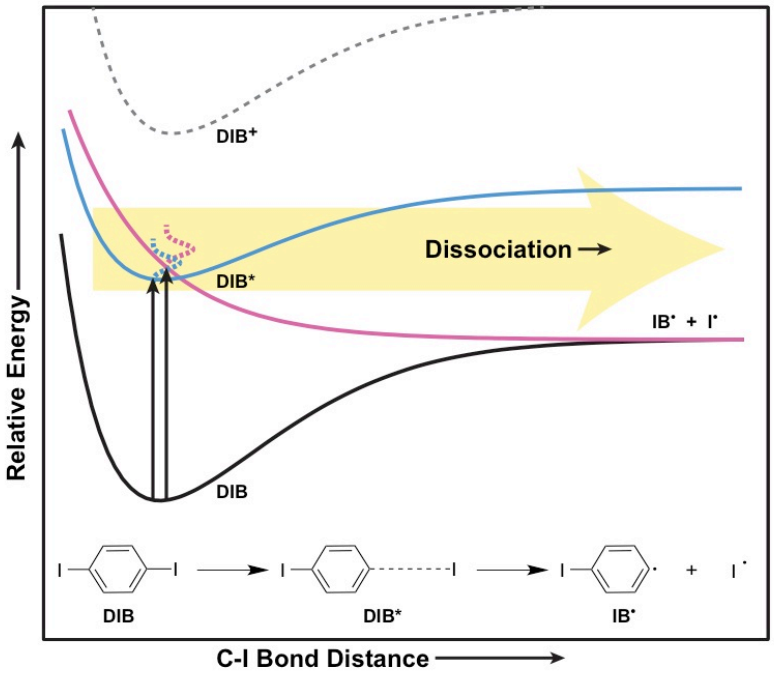

Figure 1. Illustrative schematic of the possible photodissociation pathways of DIB. The graph shows the ground and two excited state potentials corresponding to direct and indirect dissociation. The ionization potential, corresponding to the lowest DIB^+ energy, is also included (dashed line).

The present investigation aims to explore the time-resolved reaction dynamics of DIB, illustrated in Figure 1, including the initial excitation and subsequent wavepacket dynamics. By combining femtosecond spectroscopic and x-ray scattering experiments with high-level calculations of potential energy surfaces, we aim to map both the electronic and structural dynamics as a function of time. In this manuscript chronicling our initial results, we focus on the nature and lifetime of the initially excited state. Understanding this initial excitation establishes the starting point for the reaction, which is a prerequisite to understanding the mechanism of the subsequent electronic and structural dynamics. In addition, the character of the initially excited state will reveal the temporal relationship between the electronic excitation and the initiation of structural dynamics, as is required to allow for a direct comparison of spectroscopic and scattering experiments.

Experimental and Computational Approaches

The ultrafast photodissociation of 1,4-diiodobenzene (DIB) is investigated experimentally using pump-probe methodologies. In the first step, excitation at 267 nm launches a wavepacket on the excited-state surface. The nature of the excited-state surface and the related wavepacket dynamics govern the timescale of the photodissociation reaction. In the second step, the progress of the reaction is probed at variable time delays. We use two complementary approaches to illuminate the reaction from very different vantage points.

In the time-resolved spectroscopy experiment, the molecule is probed via photoionization, and the kinetic energies of ejected electrons are analyzed using a time-of-flight photoelectron spectrometer. A Ti:Sapphire oscillator (Coherent, Mantis) generates ~35 fs pulses at 800 nm, seeding a regenerative amplifier (Coherent Legend Elite Duo) operating at 5 kHz. This output is split, with 10% of the light being upconverted to the third harmonic at 267 nm using nonlinear optical crystals to serve as the pump pulse. The remaining 90% of the amplifier output seeds an optical parametric amplifier (Coherent OPerA Solo) that is tuned to 300 nm, which serves as the ionizing probe pulse. The laser pulses perpendicularly intersect a molecular beam generated by expanding a gas mixture of ~7 torr of DIB in ~850 torr of helium through a 100 μm diameter nozzle and a 210 μm diameter skimmer. By delaying the probe pulse relative to the pump pulse, we measure the kinetic energy of the ejected electrons as a function of time. The instrument response function was determined by measuring the two-color photoionization signal of acetone, which has a response time shorter than the temporal resolution of the experiment. Further details of the apparatus have been described in detail elsewhere[25,26].

In the scattering experiment, the time-evolving molecule is probed via x-ray scattering using ultrafast x-ray pulses generated at the Linac Coherent Light Source (LCLS)[27,28]. This apparatus has also been described in detail elsewhere[29]. The 267 nm pump pulse has a duration of 65 fs and is synchronized to the 120 Hz repetition rate pulse stream of the LCLS. Each x-ray probe pulse, with a photon energy of 8.3 keV, contains about 10^{12} photons and has a 30 fs pulse duration. For each delay time setting, the temporal jitter between the UV and x-ray pulses is monitored with <10 fs accuracy

using a specialized timing tool that has been described previously[30]. The optical and x-ray pulses are focused and combined collinearly into the diffraction chamber, which was heated to 90°C and contained less than 0.5 torr of DIB. The scattering pattern in the range of 1.0 to 4.2 $Å^{-1}$ is measured using a CSPAD[31]. The ultrafast optical pump, x-ray probe technique was previously implemented with great success in the study of the ring-opening of 1,3-cyclohexadiene[32,33]. Given the complexity of the DIB system, to date we have been able to investigate only the angular dependence of the scattering signal after the dissociation is complete. This is a first and necessary step for a more comprehensive study that will rest on the results presented here.

It is important to note that the scattering experiments are performed on a warm, low-pressure static gas, while the spectroscopic experiments probe the dynamics of molecules that have been cooled by a free-jet expansion. This implies that while the molecules in the scattering experiments are in thermally populated vibrational states, most all molecules in the spectroscopy experiments are in their vibrational ground state. But since the experiments by Bersohn *et. al.* showed no dependence on the excitation wavelength[6], we postulate that this difference does not invalidate the comparison of the results.

As for the computations, Complete Active Space Self-Consistent Field (CASSCF) calculations were performed using a correlation-consistent Dunning basis set of triple-zeta plus polarization quality (cc-pVTZ) for carbon and hydrogen atoms[34]. Iodine atoms were described by an effective core potential (ECP) to describe a 46-electron core, i.e. large-core [Kr]$5d^{10}$, with the larger cc-pVTZ-pp basis set of Peterson *et al*.[35] to describe the seven valence electrons. The ECP for iodine contains terms for the evaluation of spin-orbit coupling for the valence electrons.

To account for the effect of dynamical electron correlation on the predicted vertical transition properties, complete active space with second order perturbation theory (CASPT2) calculations were performed, using the implementation where the doubly external configurations are internally contracted and in which also subspaces of the singly external and internal configuration spaces are internally contracted[36]. An imaginary level shift of 0.3 hartree was employed to avoid intruder state problems and the carbon 1s orbitals were frozen in the CASPT2 calculations.

All calculations employed C_{2v} symmetry with the DIB molecule lying in the yz-plane. Following Ajitha *et al*.'s work on iodobenzene[37], two active spaces were employed for the CASSCF calculations on DIB: a fourteen electron in twelve orbital active space, denoted (14,12), and a (18,14) active space. The (14,12) space comprises the six benzene-like π orbitals and electrons and, for each iodine, the two C-I σ bond orbitals and electrons and the iodine p_x (out-of-plane) lone pair of electrons. The (18,14) space comprises all orbitals and electrons from the (14,12) space plus the iodine p_y (in-plane) lone pair for each iodine atom. The smaller (14,12) space is necessary due to an orbital rotation between a C-C σ core orbital (irreducible representation, IR, b_2) with the iodine p_y (in-plane) lone pair orbital (IR b_2) during unconstrained CASSCF optimization of the (18,14) active space's orbitals. Hence for the (18,14) active space, core orbitals were frozen, following an initial CASSCF(14,12) calculation, which places correctly the iodine p_y orbitals in the larger active space.

The geometry of the $^1A_1$ ground state of DIB was optimized at the CASSCF(14,12)/cc-pVTZ-pp level of theory. A 16 state-averaged (SA) CASSCF(18,14) wave function was used to study the ground and excited states: two roots in each IR of C_{2v} symmetry (A_1, B_1, B_2, A_2) of both singlet and triplet spin multiplicity. The CASPT2 calculation used the 16 SA-CASSCF(18,14) wave function as the reference wave function. Calculations on DIB^+ employed an analogous (17,14) active space in an 8 SA-CASSCF wave function: two roots of doublet spin multiplicity for each IR. All calculations were performed using the Molpro *ab-initio* electronic structure program[38].

Potential energy surfaces of DIB

To understand the structural dynamics and to aid the analysis of the experimental results we performed high-level computations to determine the potential energy surfaces for the relevant excited electronic states. Because of its large number of electrons, DIB is an exceedingly challenging system for sophisticated calculations.

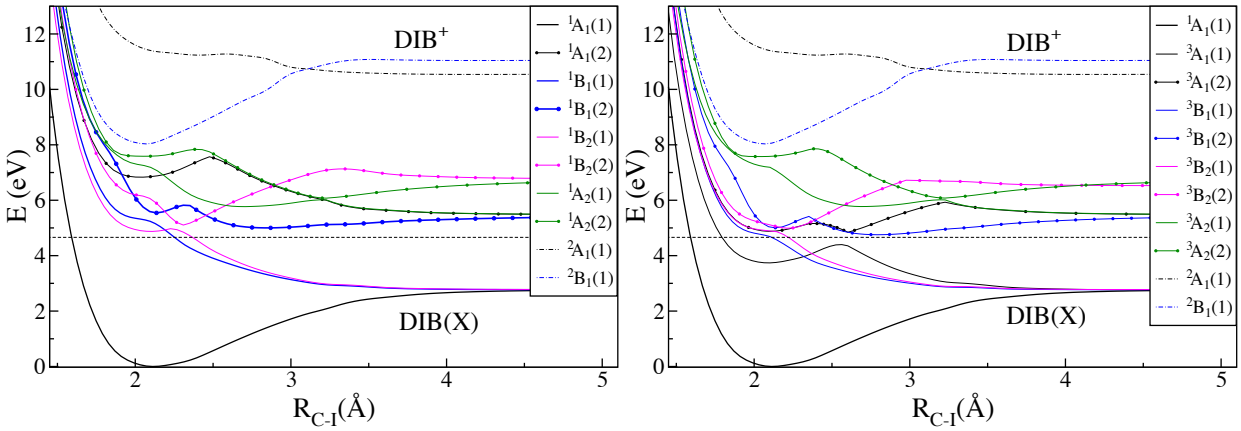

Figure 2. Computed excited-state potential energy curves of DIB at the CAS(18,14) level as a function of C-I bond distance. Singlet states (left) and triplet states (right) are plotted separately, with the $^1A_1(1)$ ground state included in both plots. The experimental excitation energy of 4.64 eV (267 nm) is marked with a straight dashed line, and the ionization limits corresponding to the two lowest energy states of DIB^+ are included as dashed curves.

	SA-CAS(18,14)-SCF			CASPT2		
STATE	**E(eV)**	**TDM (au)**	**f (au)**	**E (eV)**	**f (au)**	**Transition**
$^1A_1(1)$	0.00	0.000	0.000	0.00	0.000	–
$^1A_1(2)$	6.85	2.327	1.818	5.14	1.363	$\pi \longrightarrow \pi^*(z)$
$^1B_1(1)$	5.22	0.190	0.009	4.31	0.008	$\pi \longrightarrow \sigma^*(x)$
$^1B_1(2)$	5.57	0.312	0.027	4.41	0.021	$\pi \longrightarrow \sigma^*(x)$
$^1B_2(1)$	4.87	0.122	0.004	4.40	0.003	$\pi \longrightarrow \pi^*(y)$
$^1B_2(2)$	6.04	0.351	0.036	4.99	0.030	$n \longrightarrow \sigma^*(y)$
$^1A_2(1)$	7.18	0.000	0.000	5.89	0.000	$\pi \longrightarrow \pi^*$
$^1A_2(2)$	7.59	0.000	0.000	6.11	0.000	$n \longrightarrow \pi^*$
$^3A_1(1)$	3.74	–	–	3.64	–	–
$^3A_1(2)$	4.88	–	–	4.27	–	–
$^3B_1(1)$	4.69	–	–	3.93	–	–
$^3B_1(2)$	5.03	–	–	4.02	–	–
$^3B_2(1)$	4.89	–	–	4.20	–	–
$^3B_2(2)$	5.11	–	–	4.33	–	–
$^3A_2(1)$	7.19	–	–	5.90	–	–
$^3A_2(2)$	7.58	–	–	6.10	–	–
$^2B_1(1)$ [DIB^+]	8.05	–	–	8.43	–	–

Table 1. Vertical excitation energies, dipole transition moments (TDM), and oscillator strengths (f) for DIB at the CAS(14,12)/cc-pVTZ-pp optimized geometry with $R_{C\text{-}I}$=2.10 Å. The CASSCF calculations are performed using 16-state-averaged CAS(18,14)-SCF/cc-pVTZ-pp with ECP46, with the CASPT2 based on the CASSCF. The ionized DIB^+ ground state energy is taken from a 8-state-averaged CAS(17,14) and corresponding CASPT2 calculation. All calculations use C_{2v} symmetry. The I-I molecular axis is aligned with the z-coordinate axis, with the molecule in the yz-plane. The electronic character of each ground state to singlet excited state transition is indicated in the column 'Transitions'. Only singlet-singlet TDM's and f's are given (singlet-triplet transitions are strictly zero in the absence of spin-orbit coupling).

The calculated potential energy surfaces of DIB are shown as a function of the dissociating C-I bond distance in Figure 2. In addition, the CASPT2 calculated vertical excitation energies to the same excited states are compared with the CASSCF results in Table 1, which also includes transition dipole moments and oscillator strengths. Although the CASSCF curves are a reasonably accurate representation of the shapes of the excited states, the CASPT2 excitation energies serve as more accurate relative energies. Considering these results in combination, there are three energetically accessible singlet states. The transition dipole moments from the ground state to the $^1B_1(1)$, $^1B_1(2)$, and $^1B_2(1)$ states are computed as 0.19, 0.31, and 0.12, respectively. This indicates that the dominant transition is from the ground $^1A_1(1)$ surface to the $^1B_1(2)$ state, which has a transition dipole moment perpendicular to the molecular plane. At the excitation energy considered in this study, the $^1B_1(2)$ state is bound and dissociation can only proceed via crossing to a nearby repulsive surface. The computational results show that absorptions to the $^1B_1(1)$ and $^1B_2(1)$ states are also possible. Those

excitations have their transition dipoles oriented perpendicular to the molecular plane, and in-plane but perpendicular to the I-I axis, respectively. Excitation to the $^1B_1(1)$ state would initiate barrierless dissociation. Excitation to the $^1B_2(1)$ state would launch a wavepacket that can immediately clear a barrier, but might incur some reflection since the pump energy of 267 nm places the system only slightly above the barrier.

Energetically, there are two repulsive singlet states and three repulsive triplet states that could potentially initiate dissociation at our experimental excitation wavelength of 267 nm. Although it has not been explicitly accounted for in this calculation, it is clear that the presence of two heavy iodine atoms introduces a large amount of spin-orbit coupling, which could facilitate intersystem crossing. There are six energetically accessible triplet states in the excitation region. However, the two accessible repulsive singlet states, $^1B_1(1)$ and/or the $^1B_2(1)$, are closer in energy than any repulsive triplet to the dominantly excited $^1B_1(2)$ state, and are therefore likely most strongly coupled. The $^3B_2(2)$ state is also energetically close to the $^1B_1(2)$ state, but it is bound at this energy and would not directly initiate dissociation. It is also worth noting that the spin-orbit coupling will be critical to evaluate the asymptotic dissociation limits of the system beyond the initial early time dynamics.

The calculated potential energy surfaces suggest that the dominant decay mechanism following absorption of 267 nm radiation is predissociation. The initial excitation leads to the bound $^1B_1(2)$ state, and the dissociation occurs via subsequent crossing to the $^1B_1(1)$ and/or the $^1B_2(1)$ surface. In addition, absorption to the $^1B_1(1)$ and/or the $^1B_2(1)$ state is possible, which would lead to a direct cleavage of the C-I bond.

Time-resolved photoionization-photoelectron spectroscopy

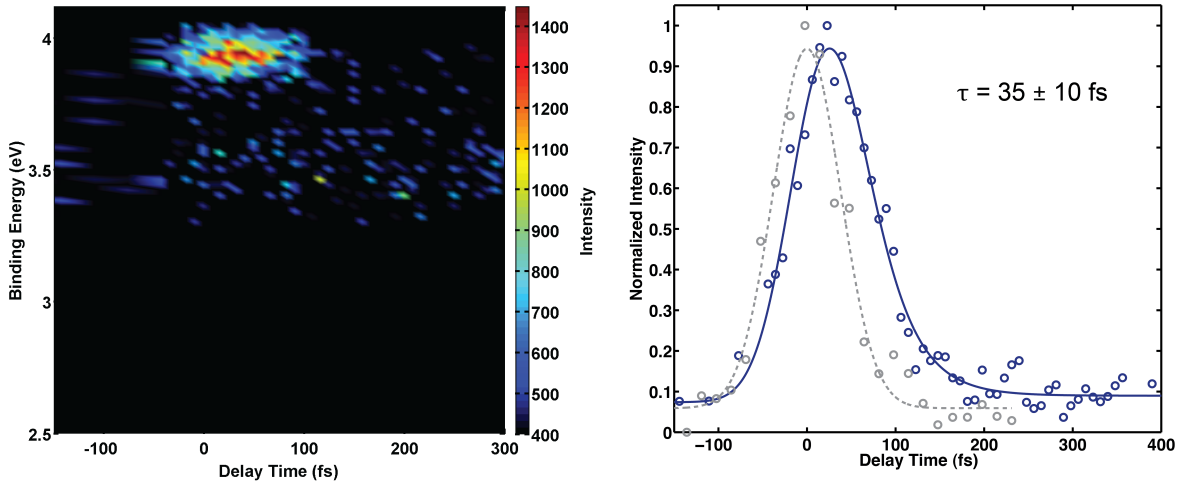

Figure 3. (Left) Two-color photoelectron spectrum of DIB, with 267 nm pump and 300 nm probe with one-color photoelectron signal subtracted. (Right) Temporal evolution of the two-color photoelectron signal centered at a binding energy of 3.94 eV (blue), and the instrument response function measured via the photoionization signal of acetone (grey). Circles represent the experimental normalized intensities, and the solid lines represent the least-squares fits.

The electronic state of DIB following excitation at 267 nm was probed via single-

photon ionization with 300 nm photons. The photoelectron spectrum shown in Figure 3 shows a single peak centered at a binding energy of 3.94 eV, which appears at time zero and quickly decays. It is apparent from the two-color photoelectron spectrum that the binding energy of the observed peak does not change as a function of time. This is suggestive of a bound electronic state, excited with vibrational energy near an energetic minimum. A repulsive surface would show a decreasing binding energy as a function of delay time. Thus, the decay of the photoelectron signal is interpreted as arising from population transfer to a nearby electronic state, likely the repulsive surface(s) that lead to dissociation.

The temporal evolution of the observed peak was fit to a single exponential decay, with time constant τ, plus a slight baseline shift at t=0. The exponential decay represents population transfer from the initially excited state (observed) to another coupled surface (unobserved). The lifetime of the initially excited state was found to be 35 ± 10 fs (all errors reported to 3σ), indicating ultrafast population transfer to a strongly coupled surface. The wavepacket is unobserved after crossing either because of a significant decrease in ionization cross-section, or because the second state quickly decreases in energy. In the present experiment, our probe energy allows for single-photon ionization of states with binding energies up to 4.13 eV.

To assign the initially excited bound state, we compare our measured photoelectron spectrum to the computed potential energy surfaces. As suggested by the computational results, initial absorption to the $^1B_1(1)$, $^1B_1(2)$, and/or $^1B_2(1)$ states is possible, with excitation to the $^1B_1(2)$ state having the highest probability. The experimentally observed signal indicates a bound state, which is consistent with absorption to $^1B_1(2)$. The $^1B_2(1)$ state also has a slight barrier and could cause partial reflection, but a significant portion of the wavepacket would likely proceed immediately over the barrier. We conclude that the observed time dependence of the spectral signature is most consistent with single-photon ionization out of the $^1B_1(2)$ state.

	Binding Energy (eV)	Transition Dipole Moment
Experiment	3.94	------
$^1B_1$ (2)	4.02	0.31
$^1B_2$ (1)	4.03	0.12
$^1B_1$ (1)	4.12	0.19

Table 2. Comparison of the experimentally measured binding energy to the CASPT2 calculated vertical binding energies and CAS(18,14) calculated transition dipole moments of the energetically accessible singlet states.

Vertical CASPT2 binding energies were obtained by subtracting the electronic excitation energies listed in Table 1 from the ionization energy. Table 2 provides a comparison of the experimentally observed binding energy with the computed binding energies of the relevant states. The experimentally measured binding energy best agrees with the computed binding energy of the $^1B_1(2)$ state. As previously discussed,

this state also has the highest computed excitation probability. Thus, the observed photoelectron signal should most likely be attributed to single-photon ionization out of the $^1B_1(2)$ state.

Additional spectroscopic signatures that could be attributed to transitions to the $^1B_1(1)$ and/or the $^1B_2(1)$ state are not observed. No significant two-color photoelectron signal was observed at the binding energy predicted for the $^1B_1(1)$ state, and no signal with a sloping binding energy (which would be consistent with excitation to the repulsive $^1B_2(1)$ state) was observed. In addition, a single exponential decay fully captures the time dependence of the observed signal, indicating that population transfer occurs from only a single electronic state. If other processes occur, they either overlap the dominant process energetically and have very similar temporal profiles, or they give significantly lower photoelectron intensity and can therefore not be observed.

X-ray scattering results

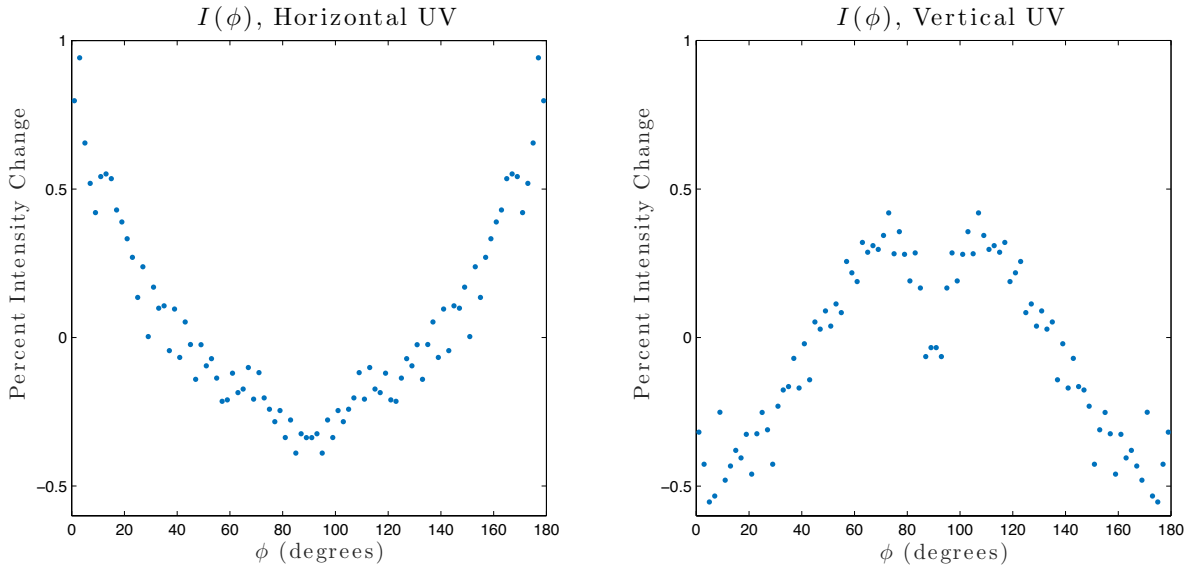

Figure 4. Overall intensity change of the x-ray scattering signal, as a function of azimuthal angle, at a time of 1 ps after excitation. The x-rays are polarized horizontally, and an azimuthal angle of 0° is defined to be the horizontal plane. Based on the symmetry of the system the signal from each quadrant must be identical and their signals have been added to reduce the noise. For visual display, the data points are plotted from 0° to 180°, so that each data point is plotted twice.

The percent difference in pump-probe x-ray scattering signal is defined as $\Delta I = 100 * \frac{I_{\text{pumped}}(\phi) - I_{\text{unpumped}}(\phi)}{I_{\text{unpumped}}(\phi)}$ where $I(\phi)$ is the sum of $I(q,\phi)$ over all observed q. This difference signal at a time of 1 ps after the photodissociation of DIB is shown as a function of the azimuthal detection angle ϕ in Figure 4. Measurements were taken with the UV pump laser polarized either horizontally or vertically, while the x-ray probe is horizontally polarized in all cases. Ejection of an iodine atom results in an oscillatory difference signal which, in an experiment with limited q range, leads to an apparent change in the scattering signal as shown in Figure 4. The dip at 90° in the plot for

vertical UV excitation is not understood yet, but might be caused by the gaps in the CSPAD detector in vertical direction. For either horizontal or vertical UV polarization, the percent difference in the scattering signal is most negative perpendicular to the direction of the respective laser polarization. This indicates that for the laser-excited molecules the I-I axis is preferentially oriented in the vertical (90°) direction for a horizontal pump and in the horizontal (0°) direction for a vertical pump, respectively. Although the anisotropy will dephase on a picosecond timescale, the preferential alignment immediately after excitation provides additional support for the nature of the initially excited state. The depletion of molecules with an I-I axis perpendicular to the UV pump pulse indicates that the transition dipole moment of the excitation must be oriented perpendicular to the I-I axis. This agrees with our assignment of the initial excitation as an absorption to the $^1B_1(2)$ state, which has a transition dipole moment oriented perpendicular to the molecular plane.

Conclusions

We present a combined experimental and computational study of the photodissociation of 1,4-diiodobenzene following excitation at 267 nm. The experimental investigations include both ultrafast time-resolved photoionization-photoelectron spectroscopy and x-ray scattering. Combined with high-level calculations, we establish the nature of the initially excited electronic state. This lays the foundation for future explorations of the electronic landscape and the reaction pathways using time-resolved photoelectron spectroscopy and x-ray scattering.

Our computational results indicate that the dominant process is the initial excitation to the $^1B_1(2)$ bound electronic state and that the dissociation must be initiated by internal conversion to one or more nearby repulsive surfaces. This finding is consistent with the photoelectron results, which indicate absorption to a bound state with a lifetime of 35 ± 10 fs. Although two other nearby singlet states were calculated to have sizeable transition dipole moments, only one excited electronic state was observed. This state was assigned as the $^1B_1(2)$ bound state because its absorption has the largest calculated transition dipole moment, and its bound character at our experimental excitation energy agrees qualitatively with the observed photoelectron spectrum. In addition, the measured binding energy of the initially excited state best agrees with the computed binding energy of the $^1B_1(2)$ state. Furthermore, our x-ray scattering results show a substantial rotational alignment of excited molecules that is consistent with the orientation of the transition dipole moment of the initial excitation.

Although several time-resolved studies of related halobenzenes have been reported[12,16,17,19,24], these experiments recorded the appearance of photofragments, leaving the lifetimes of the involved electronic states undetermined except for a qualitative comparison to rotational time scales. Dissociations faster than rotations (<1ps) are often ascribed to repulsive surfaces, while slower photofragment appearances are attributed to inherent lifetimes of an initially excited state. For example, the photodissociation of 1,4-dichlorobenzene proceeds in 122 ps and follows a predissociation mechanism[19] with the initially excited π,π* state having a lifetime of ~122 ps. Similarly, 1,4-dibromobenzene also undergoes predissociation, dissociating in

18.2 ps[17]. In contrast, our findings on DIB indicate a predissociation with a curve crossing, but on a time scale that is typically associated with a direct dissociation. This continues the trend of increased curve crossing rates with heavier halogen substitution. A similar trend has been observed for singly substituted halobenzenes.

Because the rate of curve crossing increases for heavier halogens, the effect has been attributed to intersystem crossing facilitated by spin-orbit coupling. However, our computational results indicate that the singlet repulsive surfaces are closest in energy to the initially excited state so that the mechanism in DIB is likely an internal conversion. Predissociation via intersystem crossing has not been directly observed in the other halobenzenes, but it is known that the dominant absorption leading to the photodissociation of methyl iodide is a triplet[39]. An analogous state has been assumed to initiate dissociation in halobenzenes. Instead, we find that while it is possible that a minor pathway might involve intersystem crossing, it is likely that the dominant pathway involves internal conversion.

Looking forward, we plan to investigate further the wavepacket dynamics and structural evolution in DIB upon optical excitation. Our attention will turn to a full CASPT2 calculation of the excited-state potential energy surfaces where we will attempt to incorporate state mixing via empirical spin-orbit coupling constants. Although *ab-initio* electronic structure calculations are very costly for this system, one should consider all-atom quantum molecular dynamics simulations of the photodissociation dynamics to interpret the data as fully as possible[40]. Experimentally, we will study the reaction dynamics using both time-resolved ultrafast pump-probe x-ray scattering and photoionization photoelectron spectroscopy. We expect that combined ultrafast experimental studies, such as in this article and in a prior publication[26], will become increasingly influential in interpreting complex photochemical processes, as they provide a more comprehensive signal and important cross-checks of the models used to interpret the results.

ACKNOWLEDGEMENTS

Portions of this research were carried out on the XPP Instrument at the Linac Coherent Light Source (LCLS), SLAC National Accelerator Laboratory, and were supported by the U.S. Department of Energy, Office of Science, Office of Basic Energy Sciences under Contract No. DE-AC02-76SF00515. PWM acknowledges funding by the Defense Threat Reduction Agency (DTRA), Grant No. HDTRA1-14-1-0008. BMS acknowledges funding by the NASA Rhode Island Space Grant Consortium. We also thank Jeremey Harvey for sharing the ECP46 basis set with us. The computational work used the ARCHER UK National Supercomputing Service (http://www.archer.ac.uk).

REFERENCES

[1] W. Wolf and N. Kharasch, J. Org. Chem. **26**, 283 (1961).
[2] J.A. Kampmeier and E. Hoffmeister, J. Am. Chem. Soc. **84**, 3787 (1962).

[3] A.P. Marchetti and D.R. Kearns, J. Am. Chem. Soc. **89**, 5335 (1967).
[4] A.P. Marchetti and D.R. Kearns, J. Am. Chem. Soc. **89**, 768 (1967).
[5] M. Dzvonik, S. Yang, and R. Bersohn, J. Chem. Phys. **61**, 4408 (1974).
[6] M. Kawasaki, S.J. Lee, and R. Bersohn, J. Chem. Phys. **66**, 2647 (1977).
[7] A. Freedman, S.C. Yang, M. Kawasaki, and R. Bersohn, J. Chem. Phys. **72**, 1028 (1980).
[8] T. Ichimura, Y. Mori, H. Shinohara, and N. Nishi, Chem. Phys. Lett. **122**, 55 (1985).
[9] T. Ichimura, Y. Mori, H. Shinohara, and N. Nishi, J. Spectrosc. Soc. Japan **35**, 299 (1986).
[10] H.J. Hwang and M. a. El-Sayed, J. Chem. Phys. **96**, 856 (1992).
[11] J.E. Freitas, H.J. Hwang, and M.A. El-Sayed, J. Phys. Chem. **97**, 12481 (1993).
[12] P.Y. Cheng, D. Zhong, and A.H. Zewail, Chem. Phys. Lett. **237**, 399 (1995).
[13] H.J. Hwang and M.A. El-Sayed, J. Photochem. Photobiol. A Chem. **102**, 13 (1996).
[14] G.-J. Wang, R.-S. Zhu, H. Zhang, K.-L. Han, G.-Z. He, and N.-Q. Lou, Chem. Phys. Lett. **288**, 429 (1998).
[15] R.-S. Zhu, H. Zhang, G.-J. Wang, X.-B. Gu, K.-L. Han, G.-Z. He, and N.-Q. Lou, Chem. Phys. **248**, 285 (1999).
[16] M. Kadi, J. Davidsson, A.N. Tarnovsky, M. Rasmusson, and E. Åkesson, Chem. Phys. Lett. **350**, 93 (2001).
[17] M. Kadi and J. Davidsson, Chem. Phys. Lett. **378**, 172 (2003).
[18] D. Senapati, S. Maity, and P.K. Das, J. Phys. Chem. A **108**, 7949 (2004).
[19] L.-W. Yuan, J.-Y. Zhu, Y.-Q. Wang, L. Wang, J.-L. Bai, and G.-Z. He, Chem. Phys. Lett. **410**, 352 (2005).
[20] M.D. Poulsen, E. Skovsen, and H. Stapelfeldt, J. Chem. Phys. **117**, 2097 (2002).
[21] K.-L. Han and G.-Z. He, J. Photochem. Photobiol. C Photochem. Rev. **8**, 55 (2007).
[22] X.-P. Zhang, Z.-R. Wei, Y. Tang, T.-J. Chao, B. Zhang, and K.-C. Lin, ChemPhysChem **9**, 1130 (2008).
[23] A.G. Sage, T.A.A. Oliver, D. Murdock, M.B. Crow, G.A.D. Ritchie, J.N. Harvey, and M.N.R. Ashfold, Phys. Chem. Chem. Phys. **13**, 8075 (2011).
[24] O.A. Borg, Y.J. Liu, P. Persson, S. Lunell, D. Karlsson, M. Kadi, and J. Davidsson, J. Phys. Chem. A **110**, 7045 (2006).
[25] B. Kim, N. Thantu, and P.M. Weber, J. Chem. Phys. **97**, 5384 (1992).
[26] C.C. Pemberton, Y. Zhang, K. Saita, A. Kirrander, and P.M. Weber, J. Phys. Chem. A **119**, 8832 (2015).
[27] C. Bostedt, D.M. Fritz, Z. Huang, H.J. Lee, H. Lemke, W.F. Schlotter, J.J. Turner, and G.J. Williams, Rev. Mod. Phys. **88**, 015007 (2016).
[28] W.E. White, A. Robert, and M. Dunne, J. Synchrotron Radiat. **22**, 472 (2015).
[29] J.M. Budarz, M.P. Minitti, B. Stankus, and A. Kirrander, J. Phys. B At. Mol. Opt. Phys. **49**, 34001 (2016).
[30] M. Harmand, R. Coffee, M.R. Bionta, M. Chollet, D. French, D. Zhu, D.M. Fritz, H.T. Lemke, N. Medvedev, B. Ziaja, S. Toleikis, and M. Cammarata, Nat. Photonics **7**, 215 (2013).
[31] H.T. Philipp, M. Hromalik, M. Tate, L. Koerner, and S.M. Gruner, Nucl. Instruments Methods Phys. Res. Sect. A Accel. Spectrometers, Detect. Assoc. Equip. **649**, 67 (2011).
[32] M.P. Minitti, J.M. Budarz, A. Kirrander, J. Robinson, T.J. Lane, D. Ratner, K. Saita, T.

Northey, B. Stankus, V. Cofer-Shabica, J. Hastings, and P.M. Weber, Faraday Discuss. (2014).
[33] M.P. Minitti, J.M. Budarz, A. Kirrander, J.S. Robinson, D. Ratner, T.J. Lane, D. Zhu, J.M. Glownia, M. Kozina, H.T. Lemke, M. Sikorski, Y. Feng, S. Nelson, K. Saita, B. Stankus, T. Northey, J.B. Hastings, and P.M. Weber, Phys. Rev. Lett. **114**, 1 (2015).
[34] T.H. Dunning Jr, J. Chem. Phys. **90**, 1007 (1989).
[35] K. a. Peterson, B.C. Shepler, D. Figgen, and H. Stoll, J. Phys. Chem. A **110**, 13877 (2006).
[36] P. Celani and H.-J. Werner, J. Chem. Phys. **112**, 5546 (2000).
[37] D. Ajitha, D.G. Fedorov, J.P. Finley, and K. Hirao, J. Chem. Phys. **117**, 7068 (2002).
[38] H.J. Werner, P.J. Knowles, G. Knizia, F.R. Manby, and M. Schütz, Wiley Interdiscip. Rev. Comput. Mol. Sci. **2**, 242 (2012).
and
MOLPRO, version 2012.1, a package of *ab initio* programs, H.-J. Werner, P. J. Knowles, G. Knizia, F. R. Manby, M. Schütz, P. Celani, T. Korona, R. Lindh, A. Mitrushenkov, G. Rauhut, K. R. Shamasundar, T. B. Adler, R. D. Amos, A. Bernhardsson, A. Berning, D. L. Cooper, M. J. O. Deegan, A. J. Dobbyn, F. Eckert, E. Goll, C. Hampel, A. Hesselmann, G. Hetzer, T. Hrenar, G. Jansen, C. Köppl, Y. Liu, A. W. Lloyd, R. A. Mata, A. J. May, S. J. McNicholas, W. Meyer, M. E. Mura, A. Nicklass, D. P. O'Neill, P. Palmieri, D. Peng, K. Pflüger, R. Pitzer, M. Reiher, T. Shiozaki, H. Stoll, A. J. Stone, R. Tarroni, T. Thorsteinsson, and M. Wang, see http://www.molpro.net.
[39] S.H. Gardiner, M.L. Lipciuc, T.N. V. Karsili, M.N.R. Ashfold, and C. Vallance, Phys. Chem. Chem. Phys. **17**, 4096 (2015).
[40] A. Kirrander, K. Saita, and D. V Shalashilin, J. Chem. Theory Comput. **12**, 957 (2016).